A Minimum Free Energy Model of Motor Learning

B. A. Mitchell
brian_a_mitchell@engineering.ucsb.edu
Department of Computer Science, University of California, Santa Barbara,
Santa Barbara, CA 931056, U.S.A.

N. Lauharatanahirun
nina.lauharatanahirun.civ@mail.mil
Human Research and Engineering Directorate, The CCDC Army Research
Laboratory, Aberdeen Proving Ground, MD 21005, U.S.A., and Annenberg School
for Communication, University of Pennsylvania, Philadelphia, PA 19104, U.S.A.

J. O. Garcia
javier.o.garcia.civ@mail.mil
Human Research and Engineering Directorate, The CCDC Army Research
Laboratory, Aberdeen Proving Ground, MD 21005, U.S.A., and Department of
Bioengineering, University of Pennsylvania, Philadelphia, PA 19104, U.S.A.

N. Wymbs
nwymbs@gmail.com
Department of Physical Medicine and Rehabilitation, Johns Hopkins Medical
Institution, Baltimore, MD 21205, U.S.A.

S. Grafton
stgrafton@ucsb.edu
Department of Psychological Brain Sciences, University of California,
Santa Barbara, Santa Barbara, CA 931056, U.S.A.

J. M. Vettel
jean.m.vettel.civ@mail.mil
Department of Psychological Brain Sciences, University of California, Santa Barbara,
Santa Barbara, CA 931056, U.S.A.; Human Research and Engineering Directorate,
The CCDC Army Research Laboratory, Aberdeen Proving Ground, MD 21005,
U.S.A.; and Department of Bioengineering, University of Pennsylvania,
Philadelphia, PA 19104, U.S.A.

L. R. Petzold
petzold@engineering.ucsb.edu
Department of Computer Science and Department of Mechanical Engineering,
University of California, Santa Barbara, Santa Barbara, CA 931056, U.S.A.

Even highly trained behaviors demonstrate variability, which is correlated with performance on current and future tasks. An objective of motor learning that is general enough to explain these phenomena has not been precisely formulated. In this six-week longitudinal learning study, participants practiced a set of motor sequences each day, and neuroimaging data were collected on days 1, 14, 28, and 42 to capture the neural correlates of the learning process. In our analysis, we first modeled the underlying neural and behavioral dynamics during learning. Our results demonstrate that the densities of whole-brain response, task-active regional response, and behavioral performance evolve according to a Fokker-Planck equation during the acquisition of a motor skill. We show that this implies that the brain concurrently optimizes the entropy of a joint density over neural response and behavior (as measured by sampling over multiple trials and subjects) and the expected performance under this density; we call this formulation of learning minimum free energy learning (MFEL). This model provides an explanation as to how behavioral variability can be tuned while simultaneously improving performance during learning. We then develop a novel variant of inverse reinforcement learning to retrieve the cost function optimized by the brain during the learning process, as well as the parameter used to tune variability. We show that this population-level analysis can be used to derive a learning objective that each subject optimizes during his or her study. In this way, MFEL effectively acts as a unifying principle, allowing users to precisely formulate learning objectives and infer their structure.

1 Introduction

Motor learning in biological systems is defined as a change in the capacity to behave based on experience and practice. The change in behavioral capacity is typically described in terms of improved performance. However, it has become increasingly apparent that an additional important property of movement is persistent performance variability despite extensive training. Indeed, there exists an extensive number of motor control studies of birdsong, locomotion, and limb control demonstrating the extent to which movement variability influences and is influenced by performance and learning (Haar, Donchin, & Dinstein, 2017; Wu, Miyamoto, Castro, Lvecsky, & Smith, 2014; Olveczky, Andalman, & Fee, 2005; Kao, Doupe, & Brainard, 2005; Tumer & Brainard, 2007).

An important theme throughout this letter is that even in learned, highly stereotyped behaviors, there exists variability in the expression of these behaviors within and across subjects. The presence of systematic variability in behaviors that have been heavily trained poses a problem for understanding how these systems learn. Even in the case where the behavior is generated by a stochastic system, the learning objective cannot simply be a

single performance variable such as error minimization (accuracy) or maximal speed; this would result in behavior with zero variability and suggests that a more general framework for characterizing learning objectives is necessary to explain a putative aspect of motor learning.

To address this need, we present an approach that tracks dynamic changes of performance (in our study, movement time) while also capturing performance variability in terms of a free energy functional of density dynamics. At the same time, we characterize the evolving dynamics of neural activity, whose variability is also described as a property of a density function. Neural activity is based on fMRI blood oxygen level dependent (BOLD) measurements recorded as subjects learn a set of finger sequences practiced at different training intensities. The goal of this work is to determine how the joint brain-behavior densities evolve as a function of the amount of training.

We show that the dynamics of the density over global (all brain regions) and localized (the task-active regions) brain-behavior pairs follow a Fokker-Planck partial differential equation (FPE). (We use the term *density* as shorthand for probability density function in this work.) The FPE is a fundamental aspect of the physical sciences for both classical and quantum mechanics (Kadanoff, 2000; Leal, 2012; Landau & Lifshitz, 1965). With respect to the neurosciences, the FPE is the population-level version of the drift-diffusion equation often used to model decision making (Heekeren, Marrett, Bandettini, & Ungerleider, 2004; Forstmann et al., 2008) and has also been used to model stochastic neuronal dynamics (Harrison, David, & Friston, 2005). The advantage of this joint brain-behavior density framework is that it offers a potential explanation of the nature of behavioral variability and how it is tuned during learning. A strength of this explanation is that it is grounded in the dynamics of the underlying neural activity. To the best of our knowledge, the combined modeling of neural activity and behavior is a novel extension of past work on motor variability (Haar et al., 2017; Wu et al., 2014; Olveczky et al., 2005).

The introduction of this joint brain-behavior framework provides a precise formulation of the learning objective that gives rise to the observed variability. Specifically, we show that the optimization of a popular objective in the reinforcement learning and optimal control literature (Haarnoja, Tang, Abbeel, & Levine, 2017) also yields dynamics that follow the FPE. This objective is so named because it contains two terms: *expected performance of the brain-behavior density* and its *entropy*. We refer to this framework as minimum free energy learning (MFEL). The consequences of this finding are twofold. First, it suggests an appropriate definition of behavioral variability as the entropy of the brain-behavior density. Next, it suggests a way to recover the parameters of the MFEL objective to infer the performance objective optimized, as well as the manner in which variability is tuned during learning.
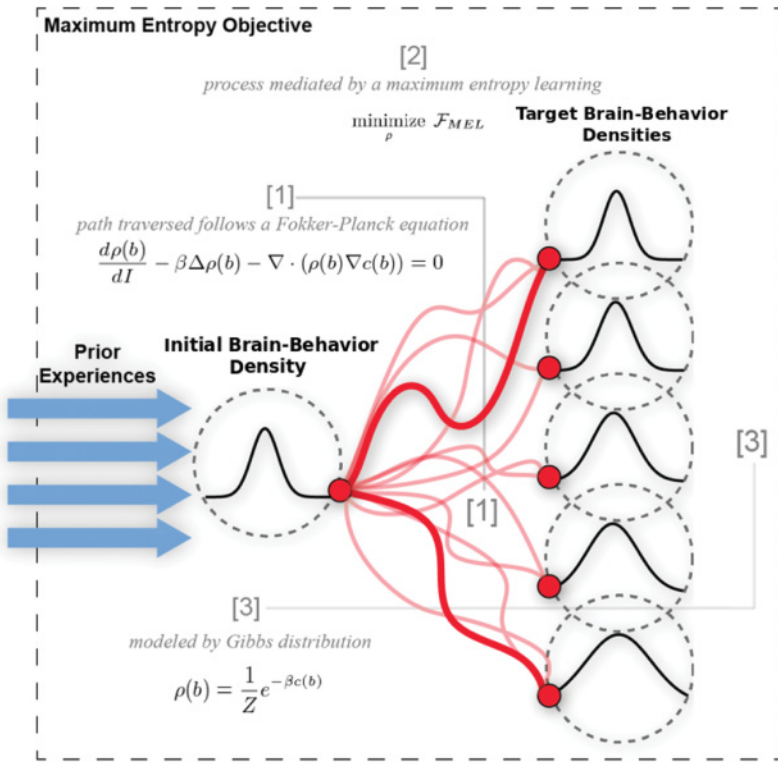
Maximum Entropy Objective

[2]

process mediated by a maximum entropy learning

$$\underset{\rho}{\text{minimize}}\ \mathcal{F}_{MEL}$$

Target Brain-Behavior Densities

[1]

path traversed follows a Fokker-Planck equation

$$\frac{d\rho(b)}{dI} - \beta\Delta\rho(b) - \nabla\cdot(\rho(b)\nabla c(b)) = 0$$

Prior Experiences

Initial Brain-Behavior Density

[3]

[1]

[3]

modeled by Gibbs distribution

$$\rho(b) = \frac{1}{Z}e^{-\beta c(b)}$$

Figure 1: Overview of the findings of this work. Previous experience is embodied in the initial brain-behavior density before any learning. Based on the form of the dynamics of this density (red lines, [1]), this density is modeled as a Gibb's distribution ([3]). The eventual target of these dynamics is largely influenced by the temperature parameter, β. This coefficient tunes the entropy of the brain-behavior density, as shown by the minimum free energy objective [2].

Using a novel variant of inverse reinforcement learning, we retrieve the cost function optimized during motor learning, as well as the parameter tuning the entropy of the brain-behavior density (see Figure 1).[1] This allows us to relate the population-level analysis performed to infer these objects to learning on the individual level. In particular, we show that the MFEL framework is appropriate to characterize individual learning by showing that individuals optimize the same objective as the population of subjects.

---

[1]The appeal to reinforcement learning is meant to highlight the connection between our method and the control of neural systems. In fact, the method presented in the online supplement is a generic approach to parameter estimation for density dynamics following the Fokker-Planck equation.
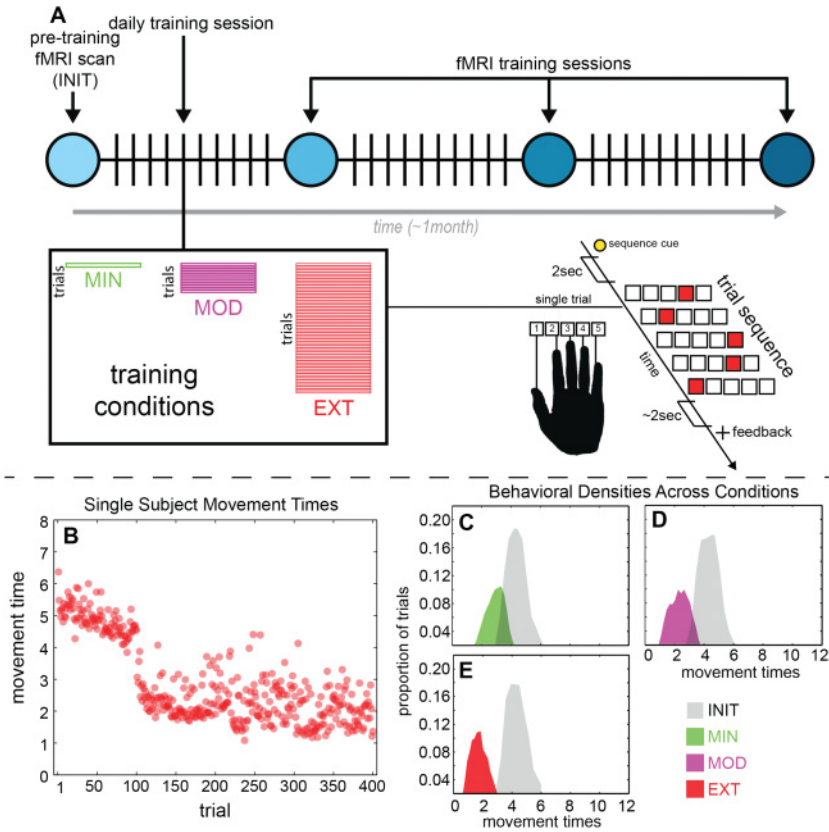
Figure 2: (A) Schematic summarizing the DSP task as well as the experimental design. (B) Example movement times for a single subject in the EXT condition. Each scanning session consists of 100 trials, and each point gives the performance on a single trial. Movement time variability persists even with the highest training intensity and duration. (C–E) Evolution of movement time densities for EXT (panel E), MOD (panel D), and MIN (panel C) conditions with INIT shown in gray.

2 Methods

2.1 Experimental Design. The motor sequence training protocol occurred over a six-week period with four MRI scanning sessions spaced two weeks apart on days 1, 14, 28, and 42 (see Figure 2). On day 1 of the experimental protocol, the participants completed their first MRI session, scan 1, and the experimenter installed the training module on the participant's personal laptop and explained how to use it for at-home training sessions.

Behavioral measurements were taken during these at-home training sessions, and interspersed throughout this training regimen, neuronal measurements were taken using fMRI BOLD. Participants were required to do the training for a minimum of 10 out of the 14 days in each two-week period between the subsequent scanning sessions. All participants completed the full training regimen; none completed fewer than 10 full training sessions.

In their at-home training sessions, participants practiced a set of 10-element sequences using their right hand. Sequences were presented using a horizontal array of five square stimuli, and the key responses were mapped from left to right, such that the thumb corresponded to the leftmost stimulus and the pinky finger corresponded to the rightmost stimulus (see Figure 2). A square highlighted in red served as the target stimulus, and the next square in the sequence was highlighted immediately after each correct key press. If an incorrect key was pressed, the sequence was paused at the error and restarted upon the appropriate key press. Participants had an unlimited amount of time to respond and complete each trial.

Each practice trial began with the presentation of a sequence-identity cue that identified one of six sequences. These six sequences were presented with three different levels of exposure in order to acquire data over a larger range of learning stages while controlling for the effect of scanning day. The two extensively trained (EXT) sequences were identified with a colored circle (cyan for sequence A and magenta for B), and they were each practiced for 64 trials during every at-home training session. The two moderately trained (MOD) sequences were identified by triangles (red for sequence C and green for D) and each practiced for 10 trials in every session. The two minimally trained (MIN) sequences were identified by black outlined stars (filled with orange for sequence E and white for F) and practiced for only 1 trial each during the at-home training sessions. Participants were given feedback every 10 trials that reported the number of error-free sequences and the mean time required to complete them.

2.2 Data Collection. Twenty-two right-handed participants (13 women and 9 men; mean age, 24 years) volunteered and provided informed consent in writing in accordance with the guidelines of the Institutional Review Board of the University of California, Santa Barbara. All had normal or corrected vision and no history of neurological disease or psychiatric disorders. We excluded 2 participants; one participant failed to complete the experiment, and the other exhibited excessive head motion (persistent head motion greater than 5 mm during the MRI scanning).

During each of the four MRI scanning sessions, we collected functional echo planar imaging data while participants performed 300 trials of the self-paced motor sequence task. Unlike the at-home practice sessions, participants completed an equal number of trials for each of the three exposure types. The 50 trials for each sequence type were grouped in blocks of 10 trials of the same sequence type (10 MIN, 10 MOD, 10 EXT), and the blocks

were randomly ordered across the five BOLD runs. After each block of 10, participants received feedback about the number of error-free sequences and mean reaction time to complete the sequences.

Because sequence production was self-paced, the number of scanned TRs varied between subject and session. In order to collect event-related fMRI data, the intertrial interval ranged between 0 and 6 s (average of 5 s). The number of sequence trials performed during each scan session was the same for all subjects with the exception of two abbreviated sessions due to technical problems. In each of these two cases, the scanning protocol was stopped short, so that four of the normally acquired five runs were completed. Data from these sessions are included in our analysis.

2.3 fMRI Data Analysis. Functional imaging data processing and analysis were performed using statistical parametric mapping (SPM8, Wellcome Department of Cognitive Neurology). Raw functional data were realigned, coregistered to the native T1 (using the first mean image as the base image for all functional scans), normalized to the MNI-152 template with a resliced resolution of $3 \times 3 \times 3$ mm, and then smoothed with a kernel of 8 mm full width at half-maximum.

BOLD response was modeled for each subject using a single design matrix with parameters estimated using a general linear model (GLM). An event-related design was used to model sequence-specific activity patterns. Trial onset is signaled by the presentation of the sequence identity cue and is presented 2 s prior to the initial discrete sequence production (DSP) target stimulus. Neural activity in this case reflects both the preparation and production of learned sequences. The design matrix for each subject was constructed using separate factors for each scan session (pretraining, training sessions 1–3), exposure condition (MIN, MOD, and EXT), and repetition (new or repeated trial). A trial is coded as a repeated event if the previous trial was the exact same sequence and the previous trial had been performed correctly. Error trials and repeated trials that followed error trials were modeled using a separate column in the design matrix. Blocking variables were used to account for nonspecific session effects for each scan run.

The full-factorial design option in SPM was used to perform higher-level mixed-effects group analysis. Skill-specific longitudinal effects were modeled using a single factor (12 levels: one for each exposure condition and session). Training intensity, that is, the cumulative number of training trials performed, was used for model factor levels: pretraining (MIN/MOD/EXT), MIN during training scans 1 to 3, MOD during training scans 1 to 3, and EXT during training scans 1 to 3. We were primarily interested in analyzing BOLD dynamics with respect to training intensity. To do this, a contrast was developed at the group level where the main effect of training intensity, over all sequences, scanning sessions, and types of training intensity, was calculated using a one-sample t-test and corrected for multiple comparisons using family-wise error (FWE) correction ($p < 0.05$).

Based on the previous literature on motor learning, we focused our analysis on nine sensorimotor regions, including the postcentral gyrus, supplementary motor area, and lateral occipital cortices (Mattar et al., 2018). To investigate neural activation within these areas during the task, we constructed a mask image representing the intersection of each brain region as indicated by the Harvard-Oxford atlas and the group level contrast of training intensity that was FWE corrected. This ensured that we analyzed the task-active voxels within the sensorimotor regions that were common across the group, and then we extracted an average time series for each individual from each region for each training intensity. This provided a matrix that was 24 (subjects) × 9 (sensorimotor regions) × 3 (training intensity MIN, MOD, and EXT).

The estimated beta weights reflect a group-level GLM contrast that reflects the main effect of training intensity across all sequences, scanning, sessions, and types of training intensity. This map was the result from a one-sample t-test corrected for multiple comparisons using a family-wise-error (FWE) correction with a p-value threshold of 0.05. The higher-level group mixed-effects model was estimated using all but one subject, and from this, the identified local optima were used to extract mean beta weights from the remaining subject. Mean beta weights were extracted using a spherical ROI (6 mm radius) centered on each local optimum. We performed this procedure for each of the 20 subjects, so that the displayed amplitudes correspond to the overall mean of the left-out-subjects' beta weights.

The brain regions outside the sensorimotor system were defined based on task active voxels in the group-level contrast, reflecting the main effect of training intensity across all sequences, scanning sessions, and types of training intensity. A mask image was constructed that represented the intersection of each Harvard-Oxford anatomical region and the group-level task activation image, and then the mask was applied to each subject's image. For each subject, the mean of the extracted, nonzero voxels within each region for each subject and each condition was computed.

3 Results

In our longitudinal study of motor learning, participants ($N = 20$) performed a discrete sequence production task for six weeks where we varied the amount of practice across a set of six sequences. Neural responses (BOLD activity) were recorded to obtain baseline neural responses while the participants were first being exposed to the sequences (INIT). As shown in Figure 2A, participants then completed at-home training sessions where two of the sequences were trained extensively (64 trials per session; EXT), two were trained moderately (10 trials per session; MOD), and two minimally (1 trial per session; MIN). Performance was measured by movement time to complete the sequence where the subjects were instructed to prioritize perfect accuracy over completing the movement sequences faster.

Across the four imaging sessions (with two weeks' separation between each), whole-brain analysis was conducted to identify brain regions activated during sequence production for each training intensity condition. Beta values (derived from modeling BOLD activity using a GLM) from whole brain analysis were extracted using the Harvard-Oxford atlas. Density estimates were constructed from histograms of beta values using evenly spaced bins over the support of the distribution. These distributions were constructed using measurements taken from all subjects, trials, and brain regions for a given condition (INIT, MIN, MOD, or EXT).

3.1 Behavioral Variability Persists during Motor Learning. First, we examine behavioral performance during a motor learning task as a function of training intensity. Across all participants and all training intensity conditions, there was a reduction in movement time during the motor learning task (see Figures 2C to 2E). A significant decrease in average movement time across all training intensity conditions relative to the initial training session was observed (see Figure 2C; MIN versus INIT, M = 1.88, SD = 0.63, t(df) = 139.83, p < 0.0001; MOD versus INIT, M = 2.49, SD = 0.75, t(df) = 96.86, p < 0.0001); EXT versus INIT, M = 3.04, SD = 0.71, t(df) = 74.65, p < 0.0001), with average performance on sequences in the EXT condition showing the greatest reduction in movement times relative to initial training. In fact, alternative hypotheses were rejected using t-tests when all pairs of the four conditions were compared with each other rather than just comparing MIN, MOD, and EXT conditions with INIT (p-values were less than 0.0001). This demonstrates that the exposure of individuals to more intense training will improve their performance as defined by the average movement time.

In addition to improved average performance, motor learning is characterized by the persistence of behavioral variability. We refer to this variability as the entropy of the behavioral density. This definition is formally justified in section 3.3. The experimental data (Figure 2B) suggest that analyzing the dynamics of the density over movement times, and its entropy in particular, may help to explain the origin of this variability and allow us to understand its evolution over time.

To this point, the evolution of the movement time densities as a function of training intensity is shown in Figures 2C, 2D, and 2E. Notably, the entropy in the movement time density does not decrease to zero with increased training intensity. We relate this result to past work where even highly trained, stereotyped behaviors retain a certain amount of variability when executed (Haar et al., 2017; Wu et al., 2014; Olveczky et al., 2005; Kao et al., 2005; Tumer & Brainard, 2007). The fact that the entropy of the movement time density after high training intensity is nonzero suggests that learning has at least two objectives: improved average performance and tuning the entropy of the density. This follows from the fact that simply optimizing for average performance would result in deterministic behavior (i.e., a movement time density with zero entropy). This is not to say that
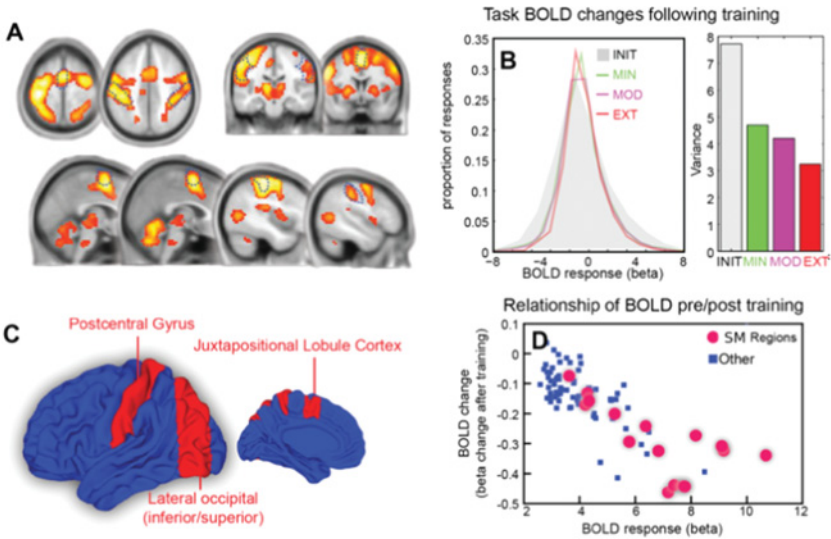
Figure 3: (A) Global task-active beta coefficients illustrated on axial, sagittal, and coronal slices (FWE < 0.05). (B) Global density of beta coefficients (left) and the variances of the densities for each training intensity. (C) Sensorimotor (SM) brain regions (red) and all other brain regions (blue). (D) Change in beta coefficient with training intensity plotted against initial beta coefficient for SM regions (red) and all other task-active regions (blue).

behavioral variability is intentionally preserved by the brain, but it may be that there is a minimum amount of noise in the execution of movements that cannot be further refined. Yet even in this case, in order to accurately model motor learning, this persistent noise must be mathematically formulated and incorporated into the model.

3.2 Motor Learning Follows Fokker-Planck Dynamics. To examine the dynamics of the neural substrates of motor learning across all regions involved in sequence production, BOLD beta values from task-dependent brain regions were extracted using the Harvard-Oxford atlas. In Figure 3, the densities of BOLD beta values are plotted to demonstrate the changes in global brain dynamics across the different training intensity conditions. There was a decrease in the entropy of the BOLD density relative to initial training, but similar to behavioral performance results, this entropy remains nonzero at the highest training intensity (see Figure 3B; INIT, $M = 0.19$, $SD = 2.78$; MIN versus INIT, $M = 0.007$, $SD = 2.16$, Levene $= 6.47$, $p = 0.012$; MOD versus INIT, $M = 0.0168$, $SD = 2.05$, Levene $= 8.50$, $p = 0.004$); EXT versus INIT, $M = 0.086$, $SD = 1.81$, Levene $= 15.14$, $p = 0.0001$).

Importantly, brain regions that are implicated in sensorimotor function are more sensitive to these dynamics than other task-relevant brain areas. This is shown in Figure 3D, where the change in the beta coefficient with increased training intensity is plotted against the initial beta coefficient, and a two-dimensional Kolmogorov-Smirnov test distinguishes these two groups of brain regions with p-value of 0.00031. This result also holds at the individual level for all but four subjects (with p-values of 0.05926, 0.11123, 0.18631, and 0.11049, respectively).

Naively, this decreasing entropy seen at the global scale might be explained by a minimization of extraneous and error-prone movements and a refinement of movements to more efficiently execute each sequence. But the dynamics of the movement time density in Figures 2C, 2D, and 2E suggest that the influence of training intensity is more subtle. Simply optimizing for performance (movement time) would result in deterministic behavior. The fact that even expert behavior on EXT sequences is probabilistically distributed suggests that a different model of learning is required.

To better visualize the relationship between neural activity and movement time, we plot the brain-behavior density as it evolves with increased training intensity in Figure 4. A partial differential equation (PDE) that captures the dynamics shown is the Fokker-Planck equation (FPE), which is given by

$$\frac{d\rho(b)}{dI} - \beta \Delta \rho(b) - \nabla \cdot (\rho(b)\nabla c(b)) = 0, \tag{3.1}$$

where b is the 2-tuple containing the random variables for neural activity and behavior, $\rho(b)$ is the probability density over brain-behavior pairs, Δ is the Laplacian operator, $\nabla\cdot$ is the divergence operator, $c(b)$ is a cost function, β is the diffusion coefficient, and I is the training intensity. This equation can be understood as shifting an initial value of $\rho(b)$ (corresponding to the INIT condition) in the direction specified by $\nabla c(b)$ while producing diffusion, the direction and rate of which is specified by β (we relate the diffusion of $\rho(b)$ to entropy in the next section). We have defined the evolution of the density with respect to training intensity, though the FPE is typically used to characterize the evolution of a density with respect to time. Since we have also defined training intensity as the number of exposures of a subject to a sequence, assuming each exposure takes a fixed amount of time, these two approaches can be seen as equivalent.

In the case of the DSP task presented in this work, the cost function is the mathematical representation of the motivation each subject has to improve his or her respective performance on the task. Put simply, $\rho(b)$ performs steepest descent on $c(b)$ to improve performance and change the shape of $\rho(b)$, while the diffusion term tunes the entropy of $\rho(b)$. The incorporation of this function into the FPE framework not only gives insight into the dynamics of the brain-behavior densities (goodness-of-fit tests are provided
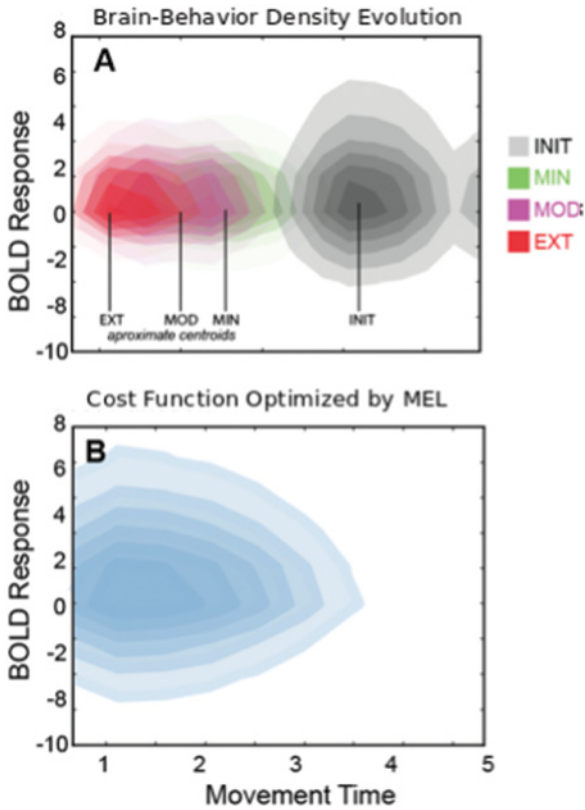
Figure 4: (A) Evolution of the brain-behavior densities with increased training intensity. (B) The cost function optimized during MFEL as derived from population-level analysis.

in the supplement), but also the rate at which the brain-behavior densities converge to an expert state during learning. In the supplement, we show that the solution of the FPE converges to steady state exponentially fast, explaining the exponential improvement seen in the subjects' behavioral performance.

Previous work in neuroscience and physics has demonstrated that the use of Fokker-Planck dynamics is a biologically appropriate model for explaining stochastic neuronal dynamics (Harrison et al., 2005). While a majority of prior work has primarily focused on using the FPE to model stochastic changes in neuronal networks, this study extends this line of research to explain the neurobehavioral dynamics of motor learning through training. Specifically, we extend the use of the FPE to show that it applies to

jointly model the BOLD response and behavior of subjects, a result that does not necessarily follow from past work on neuronal dynamics. In the context of motor learning, the FPE provides a mathematical framework to precisely define the source of and mechanism for tuning behavioral variability: both derive from diffusion of the brain-behavior density.

3.3 Fokker-Planck Dynamics Are Generated via Free Energy Optimization. While the FPE may capture the dynamics of the brain-behavior density during learning, it is not clear how these dynamics relate to the problem solved by the subjects. In fact, the FPE suggests a popular framework as a model for the learning problem solved by the subjects. To proceed further, though, we require a model of the brain-behavior density. The steady-state distribution of the Fokker-Planck equation is the Gibbs distribution,

$$\rho(b) = \frac{1}{Z}e^{-\beta c(b)}, \tag{3.2}$$

where Z is a normalizing constant and β is a temperature parameter. This distribution also appears in the literature under the name "maximum entropy distribution." There are many ways to interpret this name, but perhaps the most direct is to begin with an optimization problem. Consider the objective

$$\mathcal{F}_{MFEL} = \mathrm{E}_\rho[c] - \beta \mathrm{H}[\rho], \tag{3.3}$$

where H is the entropy of ρ, E_ρ is the expectation operator with respect to the brain-behavior density ρ, and c is the cost as defined in the previous section. Equation 3.3 is actually a specific example of a more general expression (Ortega & Braun, 2010, 2013). In particular, c may be redefined as a generic "potential" or "energy," ϕ. In its current form with ϕ interpreted as a cost, this equation is commonly used for policy optimization methods in reinforcement learning and control engineering (Kappen, Gomez, & Opper, 2012; van den Broek, Wiegerinck, & Kappen, 2010; Braun, Ortega, Theodorou, & Schaal, 2011) and can be related to models of neural systems as optimizing prediction errors (Adams, Shipp, & Friston, 2013). By setting ϕ to be the negative log-likelihood of the data, equation 3.3 can also be used to derive the evidence lower bound (ELBO), used for variational inference. This objective can be incorporated into the following optimization problem:

$$\underset{\rho}{\text{minimize}} \ \ \mathcal{F}_{MFEL}. \tag{3.4}$$

If a brain-behavior density is found by optimizing this expression in a particular way, then its dynamics follow the Fokker-Planck equation (see the

supplement for derivation). Because the dynamics of the brain-behavior density follow a Fokker-Planck equation during motor learning, equation 3.4 is also a good model of the optimization problem that accounts for the neural changes during learning. This connection formalizes the intuition given in the previous section: motor learning proceeds by simultaneous optimization of expected cost and the brain-behavior density. We refer to this model as minimum free energy learning (MFEL) throughout the rest of this letter.

The MFEL model implies that behavioral variability is tuned by adjusting the entropy of the brain-behavior density (i.e., tuning β). For example, if the entropy of the brain-behavior density is increased along the behavioral coordinate, then samples from this density are going to be more variable. Given empirical examples of the evolution of the brain-behavior density, though, it is not immediately clear how to estimate the cost function, $c(b)$, or the temperature parameter, β. These objects are retrieved in the next section (the methods for doing so are presented in the supplement), and the use of the MFEL framework as a model for motor learning is further validated.

3.4 Each Subject Learns the Same Optimal Behavior. The objective given in equation 3.4 represents a rule governing how the population of subjects learns. But when analyzing the learning procedure of individual subjects, both the structure of the brain-behavior density and its dynamics might seem quite different from those presented in Figure 4. In order to validate the utility of the population-level analysis for modeling learning within individual subjects, we first inferred the structure of the cost function optimized during motor learning. To do this, we developed a novel approach to inverse reinforcement learning (IRL) in order to compute an explicit representation of the cost function. One class of IRL methods, called maximum entropy IRL (MEIRL), attempts to infer $c(b)$ given samples from $p^*(b)$, assuming that $p^*(b)$ has the form of the Gibb's distribution. One strategy for finding $c(b)$ in this case is to use a gradient-based method to optimize the negative log likelihood of the samples (Finn, Levine, & Abbeel, 2016). This approach is not ideal in the case of the data presented here because the optimization scheme does not necessarily preserve the Fokker-Planck dynamics observed during learning. Instead, we would like to develop a method that not only retrieves $c(b)$ but does so in a way that is consistent with the dynamics of neural learning.

The method we develop relies on the modification of a popular method used to simulate the FPE. Briefly, this method simulates the FPE by solving a sequence of optimal transport problems. That is, one can simulate the FPE by, at every time step t, evolving $p_t(b)$ to $p_{t+1}(b)$ by finding the $p_{t+1}(b)$ that is as close as possible to $p_t(b)$ while still reducing the value of equation 3.3. Since for our data, $p_{t+1}(b)$ is known (i.e., it is either the empirical densities for the MIN, MOD, or EXT conditions), we simply need to solve the optimal transport problem between $p_t(b)$ and $p_{t+1}(b)$. The cost function optimized
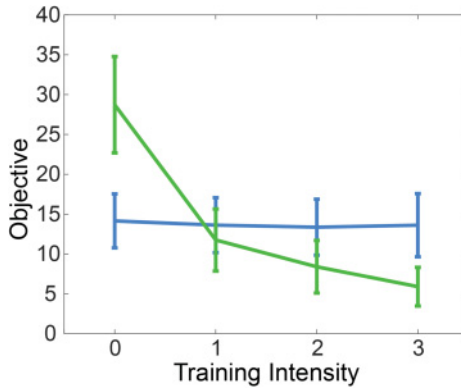
Figure 5: The value of the population-level objective for each subject plotted against training intensity (green) compared with a null model (blue). The null model was generated by shuffling data across conditions, within each subject's data set. The brain-behavior density for each subject is evaluated using the MFEL objective, where the cost function is derived from a population-level analysis. This plot demonstrates that individual subjects optimize the population-level objective.

in moving from $p_t(b)$ to $p_{t+1}(b)$ can be retrieved from the solution of these optimal transport problems (see the supplement for full derivation).

The cost function returned by our method is shown in Figure 4. The cost function is approximately convex, and this result implies, given the MFEL model, that the optimal brain-behavior density is always achieved and this density is unique. With respect to tuning behavioral variability, this theoretical guarantee indicates that there is an optimal level of variability (i.e., an optimal value for the entropy of the brain-behavior density). This follows from the fact that this cost function includes β from equation 3.2. So in effect, it includes information on the cost function being optimized, as well as the target variability.

Finally, in Figure 5, we present evidence demonstrating that each subject optimizes a similar objective. Using the cost function derived from the population-level analysis (shown in the bottom plot of Figure 4) in the objective in equation 3.4, we computed this objective using the brain-behavior densities for each individual subject. The curves presented in Figure 5 demonstrate exponential improvement in this objective with increased training intensity. Moreover, we note that nearly every subject demonstrated strictly monotonic improvement in this objective with increased training intensity. These results suggest that the estimate of the objective given in equation 3.4 is not only a good representation of population-level learning but also of learning that takes place within the individual.

4 Discussion

In this letter, we presented a minimum free energy model of motor learning. We have taken a popular objective from the engineering and statistics community, equation 3.4, and shown that it has a strong biological foundation. This connection between biology and engineering follows from the evolution of the empirical brain-behavior density according to a Fokker-Planck equation. We show how learning is characterized as evolving with training intensity and analyze the full density of observed responses (behavioral and neuronal) to justify this perspective. In doing so, we are able to connect a number of seemingly disparate schools of thought: the brain as a controller, inference engine, and dynamical system (Friston, 2010; Friston, Mattout, & Kilner, 2011; Friston, Samothrakis, & Montague, 2012). Optimization of equation 3.4 is commonly used to perform policy optimization for control systems. This problem is equivalent to the one solved during variational Bayesian inference, where the cost (c) is interpreted as a negative log likelihood and a KL divergence is minimized between estimated and actual posterior densities. And we show that if equation 3.4 is solved in a particular manner, the dynamics follow the FPE. The ability of the MFEL to act as a unifying principle across these three schools of thought allows us to lend support to the theory of learning in the brain as performing Bayesian inference. The brain-behavior densities for a given training intensity can be interpreted as posterior densities where responses are sampled from these densities. The fact that this kind of inference is performed by optimizing the entropy of Bayesian beliefs about responses speaks to the close connection between the minimum free energy and Occam's principles.

The fundamental finding that motor learning can be modeled with an FPE explains why it proceeds exponentially fast, as well as suggests a new approach to solving the IRL problem. Many different approaches to IRL have been taken, but it is not clear how any of them relate to the dynamics of learning. This raises issues related to the accuracy of the cost function retrieved, especially in the case where the solution is not unique. Our approach, based on optimal transport, is both novel and has a clear connection with the biology of learning. While optimal transport has been used for Bayesian inference, it has not been used for IRL (Moselhy & Marzouk, 2012). More important, we are able to use the population-level inferences and show that individual subjects also optimize the population-level objective. We are thus able to give both theoretical and empirical support for the use of our variant of IRL.

Another conclusion following from the observed learning dynamics is that samples from the brain-behavior density become less variable with increased training intensity. This can be interpreted as a kind of inflexibility, a concept that has been studied from a number of different perspectives previously, including a network scientific perspective (Bassett et al., 2011, 2013; Khambhati, Mattar, Wymbs, Grafton, & Bassett, 2018; Reddy et al., 2018),

aging (Berry et al., 2016) and neural systems at the cellular and circuit levels (Fusi, Asaad, Miller, & Wang, 2007). With respect to artificial controllers fit using the MFEL objective, this inflexibility manifests as an inability of learned policies to handle nonstationary environments (i.e., a cost function that changes with time; Mitchell & Petzold, 2018). It is not clear, though, that inflexibility in organic neural controllers fit using the MFEL objective would be a direct consequence of exposing subjects to increased training intensity.

One complication that might arise involves the ability of organic neural systems to maintain multiple skills at once, though it is currently an open problem to train artificial neural network controllers to do the same (Kirkpatrick et al., 2017). Inflexibility is not necessarily problematic in the case of a stationary environment. Inflexibility must thus take into account the size of the space of skills a neural controller has learned and the probability of the environment to transition away from this space. Further work is required to combine these ideas with the models of MFEL presented in this letter.

The study of individual differences with respect to the MFEL model presented in this letter is another interesting avenue for future research. We showed in Figure 5 that individual subjects largely demonstrate exponential improvement in the population-level objective with increased training intensity. Within this population of subjects, though, there is a nonzero variance over the learning rate (i.e., the value λ, if the value of the objective over intensity decays like $e^{-\lambda I}$). From the models presented in this letter, it is not immediately clear how to relate MFEL models of individual learning to MFEL models at the population level. A Bayesian approach may be fruitful, where brain-behavior densities of individual subjects are assumed to belong to a family of densities with a common prior. In this case, one would expect to be able to analyze the population-level cost function to provide insight into learning the entire task and learning dynamics in general, as has been done in this work. Further insight could be drawn based on the structure of individual cost functions, though. For example, such insight would include a better understanding of why some individuals tend to have more variable behaviors than others.

References

Adams, R. A., Shipp, S., & Friston, K. J. (2013). Predictions not commands: Active inference in the motor system. *Brain Struct. Funct.*, *218*, 611–643.

Bassett, D. S., Wymbs, N. F., Porter, M. A., Mucha, P. J., Carlson, J. M., & Grafton, S. T. (2011). Dynamic reconfiguration of human brain networks during learning. *Proceedings of the National Academy of Sciences*, *108*(18), 7641–7646.

Bassett, D. S., Wymbs, N. F., Rombach, M. P., Porter, M. A., Mucha, P. J., & Grafton, S. T. (2013). Task-based core-periphery organization of human brain dynamics. *PLoS Computational Biology 9*(9).

Berry, A. S., Shah, V. D., Baker, S. L., Vogel, J. W., O'Neil, J. P., Janabi, M., . . . Jagust, W. J. (2016). Aging affects dopaminergic neural mechanisms of cognitive flexibility. *Journal of Neuroscience 36*(50), 12559–12569.

Braun, D. A., Ortega, P. A., Theodorou, E., & Schaal, S. (2011). Path integral control and bounded rationality. In *Proceedings of the IEEE Symposium on Adaptive Dynamic Programming and Reinforcement Learning* (pp. 202–209). Piscataway, NJ: IEEE.

Finn, C., Levine, S., & Abbeel, P. (2016). Guided cost learning: Deep inverse optimal control via policy optimization. In *Proceedings of the International Conference on Machine Learning*. arXiv:1603.00448v3

Forstmann, B. U., Dutilh, G., Brown, S., Neumann, J., von Cramon, D. Y., Ridderinkhof, K. R., & Wagenmakers, E. J. (2008). Striatum and pre-SMA facilitate decision-making under time pressure. *PNAS*, *105*(45), 17538–17542.

Friston, K. (2010). The free-energy principle: A unified brain theory? *Nat. Rev. Neurosci.*, *11*, 127–138.

Friston, K., Mattout, J., & Kilner, J. (2011). Action understanding and active inference. *Biol. Cybern.*, *104*, 137–160.

Friston, K., Samothrakis, S., & Montague, R. (2012). Active inference and agency: Optimal control without cost functions. *Biol. Cybernetics*, *106*, 523–541.

Fusi, S., Asaad, W. F., Miller, E. K., & Wang, X. J. (2007). A neural circuit model of flexible sensori-motor mapping: Learning and forgetting on multiple timescales. *Neuron 54*(2), 319–333.

Haar, S., Donchin, O., & Dinstein, I. (2017). Individual movement variability magnitudees are explained by cortical neural variability. *Journal of Neuroscience*, *37*, 9076–9085. doi:10.1523/JNEUROSCI.1650-17.2017.

Haarnoja, T., Tang, H., Abbeel, P., & Levine, S. (2017). *Reinforcement learning with deep energy-based policies*. arXiv:1702.08165v2.

Harrison, L. M., David, O., & Friston, K. J. (2005). Stochastic models of neuronal dynamics. *Phil. Trans. R. Soc. 360*, 1075–1091.

Heekeren, H. R., Marrett, S., Bandettini, P. A., & Ungerleider, L. G. (2004). A general mechanism for perceptual decision-making in the human brain. *Nature*, *431*, 859–862.

Kadanoff, L. P. (2000). *Statistical physics: Statics, dynamics and renormalization*. Singapore: World Scientific.

Kao, M. H., Doupe, A. J., & Brainard, M. S. (2005). Contributions of an avian basal ganglia-forebrain circuit to real-time modulation of song. *Nature*, *433*, 638–643.

Kappen, H. J., Gomez, Y., & Opper, M. (2012). Optimal control as a graphical model inference problem. *Machine Learning*, *87*, 159–182.

Khambhati, A. N., Mattar, M. G., Wymbs, N. F., Grafton, S. T., & Bassett, D. S. (2018). Beyond modularity: Fine-scale mechanisms and rules for brain network reconfiguration. *NeuroImage*, *166*, 385–399.

Kirkpatrick, J., Pascanu, R., Rabinowitz, N., Veness, J., Desjardins, G., Rusu, A. A., . . . Hadsell, R. (2017). Overcoming catastrophic forgetting in neural networks. *Proceedings of the National Academy of Sciences*, *114*(13), 3521–3526.

Landau, L. D., & Lifshitz, E. M. (1965). *Quantum mechanics*. New York: Elsevier.

Leal, G. L. (2012). *Advanced transport phenomena*. doi:10.1017/CBO9780511800245

Mattar, M. G., Wymbs, N. F., Bock, A. S., Aguirre, G. K., Grafton, S. T., & Bassett, D. S. (2018). Predicting future learning from baseline network architecture. *NeuroImage*, *172*, 107–117.

Mitchell, B. A., & Petzold, L. R. (2018). Control of neural systems at multiple scales using deep reinforcement learning. *Scientific Reports*, *8*, 10721.

Moselhy, A. T. E., & Marzouk, Y. M. (2012). Bayesian inference with optimal maps. *Journal of Computational Physics*, *231*(23), 7815–7850.

Olveczky, B. P., Andalman, A. S., & Fee, M. S. (2005). Vocal experimentation in the juvenile songbird requires a basal ganglia circuit. *PLoS Biology*. doi:10.1371/journal .pbio.0030153

Ortega, P. A., & Braun, D. A. (2010). A minimum relative entropy principle for learning and acting. *J. Artif. Int. Res.*, *38*, 475–511.

Ortega, P. A., & Braun, D. A. (2013). Thermodynamics as a theory of decision-making with information-processing costs. *Proc. R. Soc. A*, *469*, 2153.

Reddy, P. G., Mattar, M. G., Murphy, A. C., Wymbs, N. F., Grafton, S. T., Satterthwaite, T. D., & Bassett, D. S. (2018). Brain state flexibility accompanies motor-skill acquisition. *NeuroImage 171*, 135–147.

Tumer, E. C., & Brainard, M. S. (2007). Performance variability enables adaptive plasticity of "crystallized" adult birdsong. *Nature*, *450*(7173), 1240–1244. doi:10.1038 /nature06390

van den Broek, J. L., Wiegerinck, W. A. J. J., & Kappen, H. J. (2010). Risk-sensitive path integral control. In *Proceedings of the Association for Uncertainty in Artificial Intelligence*. AUAI Press.

Wu, H. G., Miyamoto, Y. R., Castro, L. N. G., Lvecsky, B. P., & Smith, M. A. (2014). Temporal structure of motor variability is dynamically regulated and predicts motor learning ability. *Nature Neuroscience*, *17*(2), 312–321. doi:10.1038/nn.3616